Journal of Non-Crystalline Solids 475 (2017) 76–84

Contents lists available at ScienceDirect

Journal of Non-Crystalline Solids

journal homepage: www.elsevier.com/locate/jnoncrysol

Structural, optical and electrical characteristics $BaSrTiO_x$ thin films: Effect of deposition pressure and annealing

Turkan Bayrak[a,b,*], Cagla Ozgit-Akgun[c], Eda Goldenberg[b,1]

[a] Institute of Materials Science and Nanotechnology, Bilkent University, Ankara 06800, Turkey
[b] National Nanotechnology Research Center (UNAM), Bilkent University, 06800 Ankara, Turkey
[c] ASELSAN Inc. – Microelectronics, Guidance and Electro-Optics Business Sector, Ankara 06750, Turkey

ARTICLE INFO

Keywords:
$BaSrTiO_3$
Tunability
Dielectric constant
Ellipsometry
Optical constants

ABSTRACT

Among perovskite oxide materials, $BaSrTiO_x$ (BST) has attracted great attention due to its potential applications in oxide-based electronics. However, reliability and efficiency of BST thin films strongly depend on the precise knowledge of the film microstructure, as well as optical and electrical properties. In the present work, BST films were deposited at room temperature using radio frequency magnetron sputtering technique. The impact of deposition pressure, partial oxygen flow, and post-deposition annealing treatment on film microstructure, surface morphology, refractive index, and dielectric constants were studied by X-ray diffraction, scanning electron microscopy, spectrophotometry, ellipsometry, photoluminescence, as well as capacitance-voltage measurements. Well-adhered and uniform amorphous films were obtained at room temperature. For all as-deposited films, the average optical transmission was ~85% in the VIS-NIR spectrum. The refractive indices of BST films were in the range of 1.90–2.07 (λ = 550 nm). Post-deposition annealing at 800 °C for 1 h resulted in polycrystalline thin films with increased refractive indices and dielectric constants, however reduced optical transmission values. Frequency dependent dielectric constants were found to be in the range of 46–72. However, the observed leakage current was relatively small, about 1 μA. The highest FOM values were obtained for films deposited at 0.67 Pa pressures, while charge storage capacity values increased with increased deposition pressure. Results show that room-temperature grown BST films have potential for device applications.

1. Introduction

Owing to their multifunctional electro-optical properties, ferroelectric perovskite thin films are attractive materials for a wide range of applications including, decoupling capacitors, infrared detectors, and microwave tunable devices, such as phase shifters, resonators, and filters [1–5]. Among the ferroelectric materials family, $BaSrTiO_x$ (BST) thin films recently received significant attention due to their potential for high performance electronic devices due to the superior tunability, low loss, room temperature (RT) operation, and additionally being lead-free tunable perovskite [6–8].

Several techniques such as radio frequency (rf) sputtering, laser ablation, chemical vapour deposition (CVD), pulsed laser deposition, molecular beam epitaxy, and sol-gel have been used to deposit BST thin films [9–18]. Each of these techniques has its own advantages and disadvantages in terms of film properties, process cost, and process compatibility for device applications. Among these methods, sputtering is a rather simple, low cost, and effective thin film growth technique which is compatible for industrial-scale production as well.

It is well known that film characteristics are strongly affected by the growth parameters such as substrate temperature, oxygen pressure and annealing [7,9,10,19]. Numerous studies on BST thin films have been reported in the recent years, however these efforts mainly concentrated on the determination of a single physical property (i.e., either the structural, optical, or electrical properties) [18–22]. Thus, it is difficult to assess and correlate material properties. Furthermore, the device reliability and efficiency with long-term stability depend strongly on the BST film microstructure, morphology, as well as optical and electrical properties, which are currently not well understood.

Crystalline phase BST films are typically obtained at high substrate temperatures (> 500 °C). Interfaces, grain structures, composition, texture, surface morphology and residual stress are the possible causes for the permittivity reduction and the leakage current problems which are developed during high temperature film growth [23–27]. Different phases of BST as a function of annealing temperature are noted by Noh et al. They proposed an alternative approach in which films are grown

* Corresponding author at: Institute of Materials Science and Nanotechnology, Bilkent University, Ankara 06800, Turkey.
E-mail addresses: t.bayrak@hzdr.de (T. Bayrak), egoldenberg@sisecam.com (E. Goldenberg).
[1] Currently: Şişecam Science and Technology Center, Gebze, Kocaeli 41400, Turkey.

http://dx.doi.org/10.1016/j.jnoncrysol.2017.08.036
Received 3 June 2017; Received in revised form 15 August 2017; Accepted 24 August 2017
Available online 04 September 2017
0022-3093/ © 2017 Elsevier B.V. All rights reserved.

at low temperatures and crystallize later in a post-deposition annealing process to improve film properties [26].

In this work, BST thin films were deposited at room temperature by rf sputtering technique on Si (100) and UV fused silica substrates. The influence of deposition parameters and post-deposition annealing on the physical properties of BST films were systematically investigated with the correlation between deposition parameters and multi-functional materials properties. In addition to the determination of film microstructure, composition, and morphology, the variation of optical constants, photoluminescence characteristics, dielectric constants, dielectric loss, and tunability were specifically addressed for further microelectronic device applications.

2. Experimental methodology

2.1. Film deposition

BST thin films were deposited on UV Fused Silica (UVFS) and Si (100) substrates at room temperature (RT) using off-plane axis VAKSIS NanoD – 4S rf magnetron sputtering system. Ar and O_2 were introduced into the system using separate lines. During the film deposition, O_2 flow to total gas flow ratio (i.e., O_2/Ar + O_2) was kept constant at 3.3%. The depositions were performed using $BaTiO_3$/$SrTiO_3$ ceramic targets (50 mm) with a constant target-to-substrate distance of 50 mm. The chamber base pressure was $< 6.5 \times 10^{-6}$ Torr (0.9 mPa). The effect of deposition pressure (P_D = 0.67, 0.93 and 1.33 Pa) on film characteristics was studied for films deposited at a constant rf power of 75 W at 13.56 Hz. Film thicknesses were kept between 100 and 150 nm, depending on P_D. The deposition conditions are summarized in Table 1.

In order to investigate the effect of post-deposition annealing on physical properties, films were annealed at 800 °C for 1 h under O_2 ambient. Annealing was performed using ATV-Unitherm (RTA SRO-704) rapid thermal annealing system, and during annealing the O_2 flow rate was kept constant at 200 sccm. The heating rate was ~10 °C/s, and the samples were taken out from the annealing chamber after the system was cooled down below 80 °C.

2.2. Film characterization

Film microstructure was examined using grazing-incidence X-ray diffraction (GIXRD) measurements, which were carried out with a PANalytical X'Pert PRO MRD diffractometer using CuKα (λ = 1.5406 Å) radiation. GIXRD patterns were recorded within the 2Theta range of 20°–80° with an incidence angle of 0.3°. Peak positions were obtained by the fitting of GIXRD data using PANalytical X'Pert High Score Plus Software. Furthermore, interplanar spacing (d_{hkl}) values for the (002) plane and the lattice parameter (a) for cubic crystals were calculated from the corresponding peak position [28]. Crystallite sizes of the annealed films were estimated from the (002) reflection using the well-known Scherrer formula by neglecting the instrumental broadening and assuming that the observed broadening is only related to the size effect [28]. Bulk film chemical compositions and bonding states were determined by X-ray photoelectron spectroscopy (XPS) using Thermo Scientific K-Alpha spectrometer with a monochromatized

Table 1
Sputtering conditions of BST thin films.

Deposition parameters	
Base pressure (mPa)	< 0.87
Deposition pressure (P_D) (Pa)	0.67, 0.93 and 1.33
O_2/(Ar + O_2) flow ratio	3.3%
RF power (W)	75
Target size (mm)	50
Target-to-substrate distance (mm)	50
Deposition duration (min)	15–20

Al Kα X-ray source (1486.6 eV). Peak analyses were performed using the Avantage Software. No restrictions were applied to spectral locations and full width at half maximum (FWHM) values. Surface morphologies of the deposited films were revealed via atomic force microscope (AFM, Asylum Research MFP-3D), and a scanning electron microscope (SEM) (FEI, Nova Nanosem 430). AFM rms roughnesses of the as-deposited and annealed thin films were measured from 1 μm × 1 μm sample scan areas.

Optical measurements were performed using a UV-VIS-NIR single beam spectrophotometer (Ocean Optics HR4000CG-UV-NIR) in the wavelength range of 250–1000 nm relative to air, and a variable angle spectroscopic ellipsometer (V-VASE, J.A. Woollam Co. Inc.) for wavelengths ranging from 250 to 1200 nm. The ellipsometric angles (Ψ and Δ) were determined at two angles of incidence (i.e., 70° and 75). The optical properties were modeled using the homogeneous Tauc–Lorentz (TL) function for a three-layer model including the substrate, film, and surface roughness, while simple grading model was added into the calculations for annealed films in order to improve the fitting quality. Best fit data were used for the determination of optical constants, film thickness "t", and the film surface roughness. If not stated otherwise, all n and k values stated in this paper correspond to values measured at 550 nm. The absorption coefficient, $\alpha(\lambda) = 4\pi k(\lambda) / \lambda$, was calculated from the $k(\lambda)$ values. The optical band gap energy, E_g, was evaluated using the spectral absorption coefficient, which is associated with direct transition photon absorption:

$$\alpha(E) = B\frac{(E - E_g)^m}{E} \tag{1}$$

where m is a power factor generally being ½ for direct band gap materials [29,30]. Assuming that m = ½, the optical energy band gap is extracted by extrapolation of the linear part of the absorption spectrum to $(\alpha E)^2 = 0$. Thin film photoluminescence (PL) measurements were carried out by time-resolved fluorescence spectrophotometer (JobinYvon, model FL-1057 TCSPC) in the wavelength range of 300–580 nm using an excitation wavelength of ~250 nm. Metal-insulator-semiconductor (MIS) capacitor structures with BST as the insulator layer were fabricated on p-Si substrates. Silver (Ag) (~80 nm) top electrodes (9.25×10^{-8} m^2) were thermally evaporated to fabricate Ag/BST/p-Si capacitors. Current-voltage (*I-V*) and capacitance-voltage measurements (*C-V*) characteristics of the test structures were measured using a semiconductor parameter analyser (Keithley 4200-SCS), which is connected to a DC probe station (Cascade Microtech PM-5). *I-V* measurements were carried out in order to estimate the breakdown voltage (V_{bd}), breakdown field (E_{bd}), and charge storage capacity (CSC = $\varepsilon_0\varepsilon_r E_{bd}$) of the BST films. Frequency-dependent dielectric properties of the fabricated test structures were measured within the 200 Hz–1 MHz frequency range at RT using Agilent E4980A Precision LCR meter. Dielectric constants (ε) of the films were calculated from $C = \varepsilon_0\varepsilon_r A / t$, where C, t, ε_0, ε_r, and A are the accumulation capacitance, film thickness, permittivity of free space, permittivity of dielectric, and the area of electrode, respectively. The electric field-induced tunability describes the ability of a material to change its permittivity by the applied electric field and is defined as:

$$n_r = \frac{\varepsilon(0) - \varepsilon(E)}{\varepsilon(0)} \tag{2}$$

where ε(0) and ε(E) are the permittivities in the absence and presence of electric field, respectively [6]. Relative tunability of the films was determined using 0.5 V dc bias. Furthermore, dielectric loss (tan(δ)) values were calculated using the conductivity (G) data obtained with LCR meter. Finally, the frequency dependent figure of merit, FOM = n_r / tan(δ), of the BST films were also evaluated.

Table 2
Bulk elemental composition of as-deposited and annealed BST thin films as determined by XPS survey scans. Data were collected after 30 s in-situ Ar etching.

P_D (Pa)	Condition	Thickness (nm)	Chemical composition
0.67	As-deposited	118	$Ba_{0.44}Sr_{0.56}TiO_{3.63}$
	Annealed	135	$Ba_{0.44}Sr_{0.56}TiO_{3.06}$
0.93	As-deposited	159	$Ba_{0.21}Sr_{0.33}TiO_{2.32}$
	Annealed	176	$Ba_{0.21}Sr_{0.33}TiO_{2.29}$
1.33	As-deposited	143	$Ba_{0.23}Sr_{0.35}TiO_{2.40}$
	Annealed	115	$Ba_{0.27}Sr_{0.35}TiO_{2.42}$

3. Results and discussion

3.1. Film microstructure, composition and surface morphology

Survey and high-resolution XPS scans of as-deposited and annealed BST films on Si (100) were obtained as a function of P_D. The data revealed the presence of Ba, Sr, Ti, and O elements in the films. Elemental compositions of the BST films are presented in Table 2. The variation of Sr/Ti and Ba/Ti concentration can be found as: 0.56 (0.67 Pa), 0.35 (0.93 Pa), 0.33 (1.33 Pa) and 0.44 (0.67 Pa), 0.21 (0.93 Pa), 0.23 (1.33 Pa), respectively. In Fig. 1, the (Ba + Sr)/Ti concentration ratios were calculated and found to be between 1 and 0.54. Its value decreased with the increasing deposition pressure from 0.67 to 0.93 Pa. Post-deposition annealing process did not affect the Ba/Sr ratio. However, it affected the oxygen content in bulk films. However, XPS analyses indicated Ti rich BST films. Excess Ti and O might form amorphous or crystalline TiO_x, which can lower the dielectric permittivity (see *Electrical properties* section) at the grain boundaries. However, it should also be noted that there were no indications of the segregation of the excess Ti to second phases such as TiO_x phase in the GIXRD patterns.

GIXRD analyses indicated that all as-deposited films were amorphous in their as-deposited states with some nanocrystallinity (not shown here), while post-deposition annealing treatment resulted in polycrystalline thin films. Fig. 2 shows the GIXRD patterns of annealed BST thin films, which indicate a cubic crystal structure with some stoichiometric variations for films deposited at different chamber pressures (ICSD reference codes: 98-009-0006, 98-015-4403, 98-016-4371). (011), (111), (002), (112), and (022) reflections were observed for all films while additional reflections that correspond to (001) and (013) planes also appeared for films deposited at high chamber pressures.

The interplanar spacing (d_{hkl}) values of the (002) planes were calculated as 0.1991, 0.1990, and 0.1971 nm, while the lattice parameter

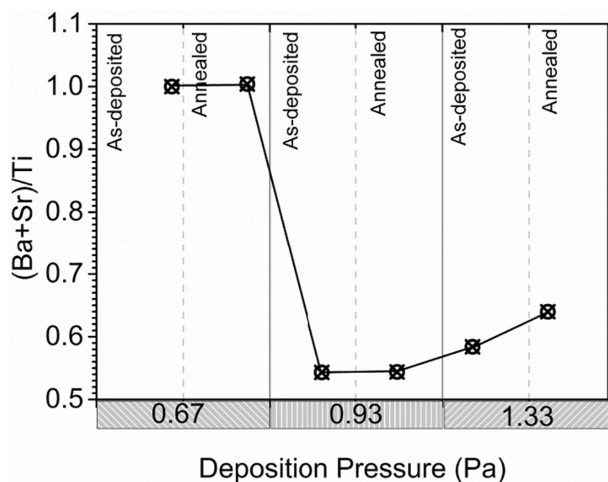

Fig. 1. (Ba + Sr)/Ti concentration as a function of deposition pressure.

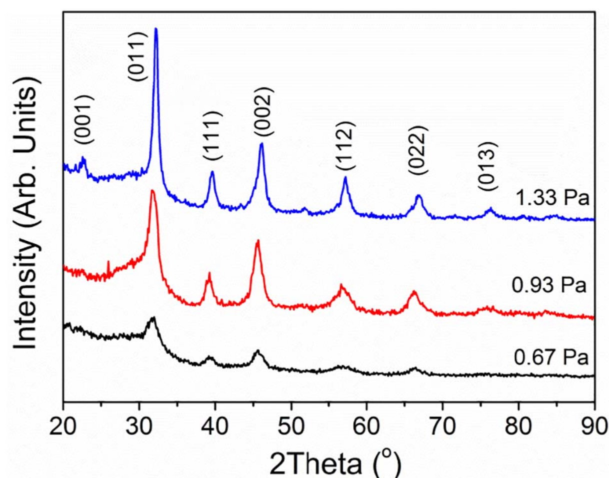

Fig. 2. GIXRD patterns of BST thin films annealed at 800 °C for 1 h under O_2 ambient.

(a) values were calculated to be 3.983, 3.980, and 3.941 Å for films deposited at a chamber pressure of 0.67, 0.93, and 1.33 Pa, respectively. The calculated lattice parameter values were in good agreement with those reported for bulk crystals. Crystallite size values were estimated from the (002) reflection using Scherrer formula and found to be ~5.8, 6.3, and 7.2 nm as a function of increasing deposition pressure. The observed crystalline size values are lower than the average of values given in literature. Singh et al. reported on the crystallinity of spin coated BST thin films as a function of annealing temperature [31]. They observed improved film microstructure with increased annealing temperatures, and higher crystallite sizes (31–40 nm) were obtained for films annealed at temperatures higher than 450 °C. In the present work, we clearly observed improved crystallinity for annealed films deposited at higher P_D; this might be attributed to the healing of oxygen vacancies. A similar material behaviour for films deposited at a higher deposition temperature (i.e., 700 °C) and oxygen pressures has also been reported by Alema et al. [32].

Surface morphologies of the films were studied using AFM and SEM. Fig. 3(a)–(c) shows the AFM 3D surface morphologies of as-deposited (P_D = 0.67 and 0.93 Pa) and annealed (P_D = 0.93 Pa) thin films. rms roughness values of the as-deposited thin films was lower for films deposited at high P_D values, being estimated as 2.13, 0.31, and 0.78 nm for films deposited at 0.67, 0.93, and 1.33 Pa, respectively. Dense and fine grained film morphology was reported by Zhang et al. for films deposited at 600 and 700 °C using rf magnetron sputtering system [29]. For annealed films, rms roughness values within the range of 6–10 nm were obtained irrespective of the deposition parameters.

As-deposited films had relatively smooth surfaces, while post-deposition annealing significantly increased the surface roughness. Plan-view SEM images of the annealed BST films, which were deposited at 0.67 and 1.33 Pa chamber pressures, are shown in Fig. 4(a) and (b), respectively. The film deposited at 0.67 Pa had a very rough surface morphology. On the other hand, for the film deposited at P_D = 1.33 Pa, void formation was observed, which might be related to the film densification and stress formation. Surface roughness values for both as-deposited annealed BST thin films were also directly calculated from spectroscopic ellipsometry analyses and results agreed well with those obtained from AFM and SEM studies. Similarly, Roy et al. also reported increased granular surface structure for films sintered at temperatures > 500 °C [33].

3.2. Optical properties

Sputtering is a well-established technique for the deposition of high quality metal oxide thin films. In this subsection we present the optical characteristics of as-deposited and annealed BST complex oxide films as

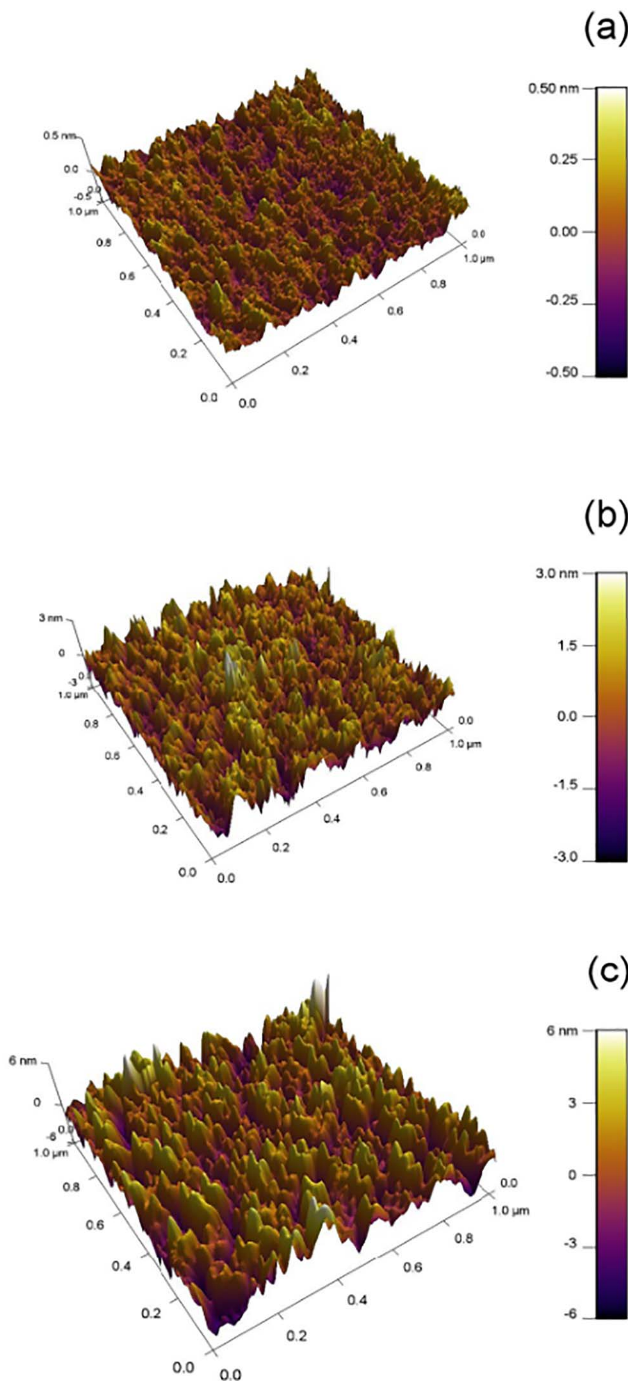

Fig. 3. AFM 3D surface morphologies of annealed BST thin films deposited at a chamber pressure (P_D) of (a) 0.67 Pa, (b) 1.33 Pa, and (c) 1.33 Pa.

a function of deposition parameters. The optical data reported here are based on spectral transmission, spectroscopic ellipsometry and PL emission measurements. In Fig. 5(a), optical transmission spectra of as-deposited BST thin films are presented for different P_D values.

The average transmissions of as-deposited films are equal to those of UVFS substrates ($k < 10^{-4}$) indicating nearly absorption-free films. Furthermore, as can be seen from the main band gap absorption edge, the film band gap does not differ from each other. However, annealing at 800 °C for 1 h, slightly lowered the level of transmission, indicating weak absorption ($k \geq 2 \times 10^{-2}$) or light scattering, which is generally increasing with crystallite size and surface roughness, as also confirmed by XRD, AFM, and ellipsometry measurements, respectively (see Fig. 5(b)). Increased light scattering with the annealing at crystal boundaries is mainly causing the optical loss. The decrease in film transmission with annealing was more pronounced for films deposited at high P_D (see inset of Fig. 5(b)). We also observed a decrease in film thickness with post-deposition annealing (as also indicated by a shift in the interference maxima). This reduction is associated with evaporation and/or densification of the films. In contrast, the increase of optical transmission is reported by Panda et al. as a function of substrate temperature for films deposited by rf sputtering [34]. Films deposited at higher substrate temperatures showed higher transmittance with lower interference oscillation, indicating lower thickness. Our observations showed that the film crystallinity increases at high temperatures and are comparable to the reports [16–21,31,33].

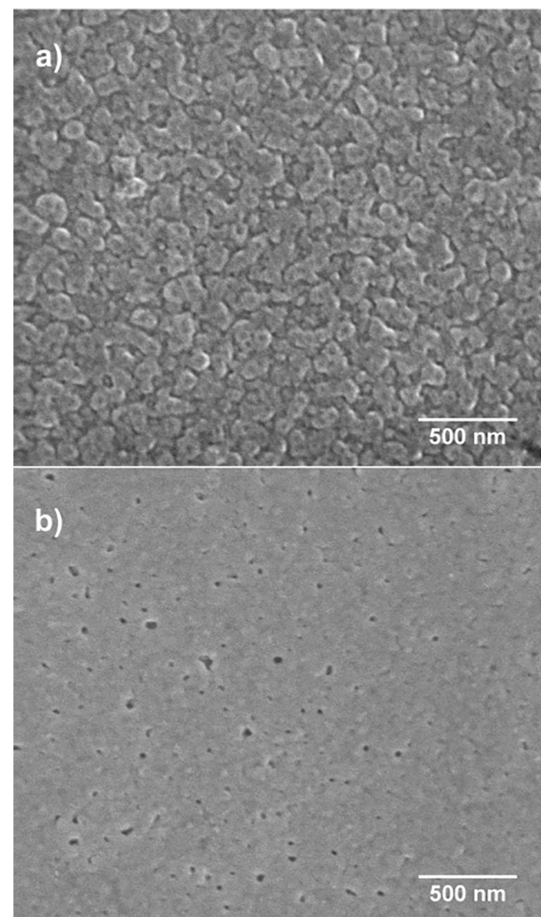

Fig. 4. Plan-view SEM images of annealed BST thin films deposited at a chamber pressure (P_D) of (a) 0.67 Pa, and (b) 1.33 Pa.

Optical constants of the films were estimated by the analysis of spectroscopic ellipsometry data. Fig. 6(a) and (b) presents examples of ellipsometric data fitting, showing the measured and calculated ellipsometric angles psi (Ψ) and delta (Δ) at the incident angles of 70° and 75° for the film deposited at 0.93 Pa.

From the calculated fit, film thickness was found to be 157.8 nm (MSE was 3 for data taken at 70° and 75°). The MSE values for the fitting of Ψ and Δ were in the range 2–9 for all BST films. Optically determined surface roughness of the films were systematically below 1.5 nm for as-deposited films, while post-deposition annealing increased surface roughness significantly up to ~16 nm. In Fig. 7(a), refractive index (n) values are given as a function of wavelength for different P_D. As seen from this figure, the dispersion curves rise rapidly towards shorter wavelengths. The strong increase in n at shorter wavelengths is associated with the fundamental band gap absorption (see Fig. 5(a) and (b)). For as-deposited BST films the refractive index decreases with P_D from 1.96 to 1.90. The decrease or increase of the

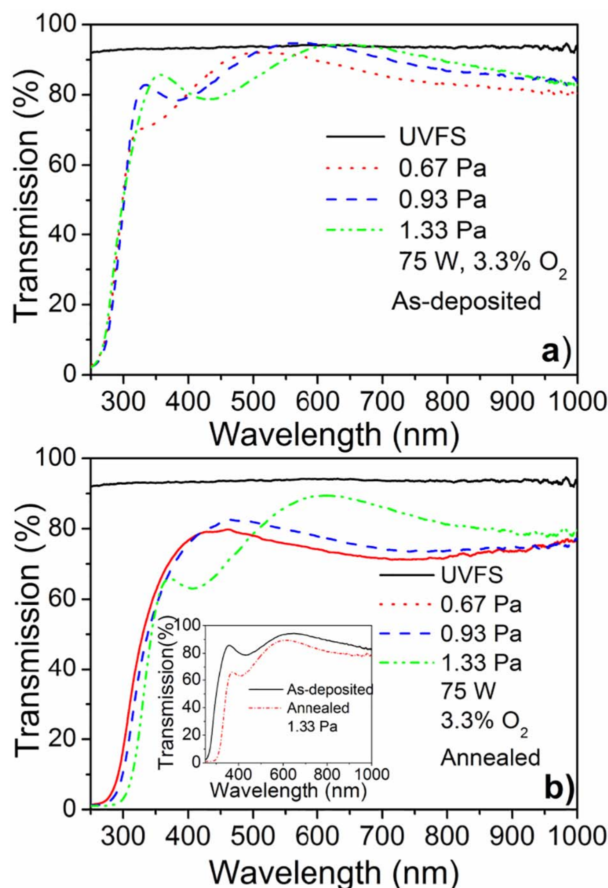

Fig. 5. Spectral optical transmission plots of (a) as-deposited, and (b) annealed BST thin films as a function of P_D. (Inset) The difference between the spectral transmission plots of as-deposited and annealed films (P_D = 1.33 Pa).

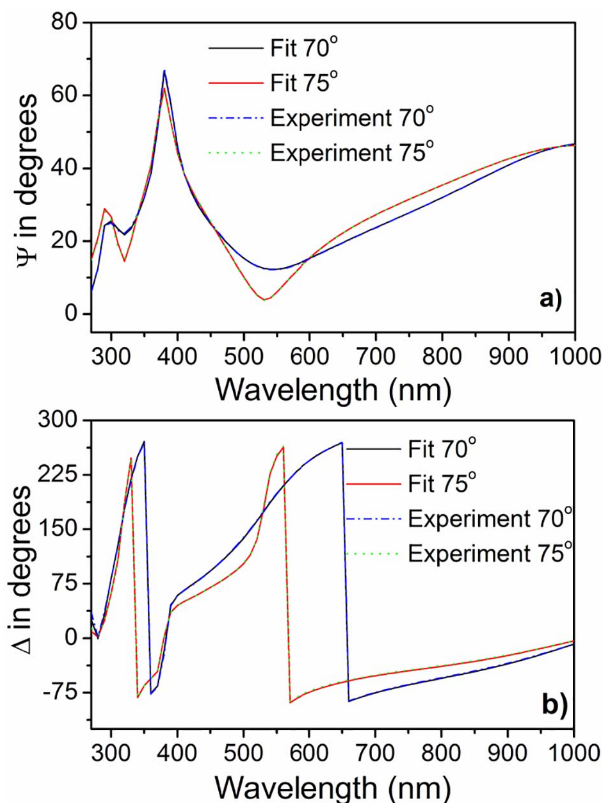

Fig. 6. Plots of measured ellipsometric data and model fit for the film deposited at PD = 0.93 Pa: (a) Ψ and (b) Δ.

refractive index results from the different effects during the sputtering process. It is generally accepted that during the deposition process, sputtering atoms/ions are scattered when the pressure is increased, and hence less dense films can form with various defect structures [8].

The effect of post-deposition annealing on n are presented in Fig. 7(b) for films deposited at 0.67 and 1.33 Pa. n values increased with annealing from 1.96 to 2.00 for the film deposited at 0.67 Pa, and from 1.90 to 1.98 for the film deposited 0.93 Pa, while a significant increase from 1.90 to 2.07 was observed for film deposited at 1.33 Pa. Refractive index, n of an oxide thin film might be directly correlated to its packing density and microstructure [8,9,35,36]. It should be noted that in the present case, amorphous films (as-deposited) exhibited lower refractive indices indicating less dense films; while the post-deposition annealing lead to denser films, resulting with an increase in the refractive index due to crystallization.

In Fig. 7(c), we present the distribution of n at λ = 550 nm for a graded film deposited at P_D = 1.33 Pa. The bulk was divided into 11 layers in depth, and the total fitting was done by fitting the optical constants in each individual layer. The relative values of n increases from 1.78 to 2.32, which might be related to the formation of an interface layer between SiO_2 and BST. It is well known effect that film refractive index is also increases with film stress hence formation of graded film structure and higher refractive index might be the result of stress formation. In addition, the segregation of the excess Ti to second phases at grain boundaries might cause graded structure. Furthermore, the optical band gap of a thin film is defined by the extrapolation of linear part of the absorption spectrum to $(\alpha E)^2 = 0$. In Fig. 7(d), $(\alpha E)^2$ vs. E plot is presented for as-deposited BST films (P_D = 0.93 Pa). The optical band gap of the as-deposited film was higher (i.e., ~4.30 eV) compared to that of bulk BST (~3.4 eV). Table 3 summarizes the optical constants and energy band gap values. A significant reduction in optical band gap was observed after post-deposition annealing. The E_g value of the film deposited at P_D = 1.33 Pa (i.e., 3.60 eV) was found to be close to the bulk value, whereas films deposited at lower pressures showed slightly higher values. Similar high optical band gap as a function of deposition parameters such as pressure, substrate temperature, and post-deposition annealing were reported in the literature [36,37]. It is known that in polycrystalline thin films, structural imperfections/defects, such as the presence of mechanical stress due to lattice distortion in the grain boundaries, and oxygen vacancies might influence the electronic structure and thereby affect the optical band gap; hence, our results might be reflecting these effects as well.

The room-temperature PL spectra of BST films deposited on Si substrates at RT and later annealed at 800 °C for 1 h are presented in Fig. 8(a) and (b). An excitation wavelength of 250 nm was used for the measurements. Fig. 8(a) shows that the all three spectra exhibit a broad spectral feature centred at 337 nm, which results from the main band gap emission. Also, the PL intensity slope is less steep within the 375–450 nm spectral regions, which might be designated to the bulk and surface related impurity and/or defect structures.

Spectral PL emission plots are presented for annealed BST films in Fig. 8(b). The emission intensities decrease with annealing, and do not differ for films deposited at different P_D. It is widely accepted that the post-deposition annealing treatment leads to an overall reduction in the defect-related luminescence, and improves film crystal quality (which is also revealed by GIXRD, see Fig. 2). However, in the present case, the PL emission intensities decreased upon annealing. Similar results were reported for ABO_3-type perovskites including $SrTiO_3$, $BaTiO_3$, and BST [36,37]. It is known that visible emission in perovskites is mainly due to their structural disorder. The localized electronic levels between the valance and conduction bands produce a disordered phase in structural symmetry [38].

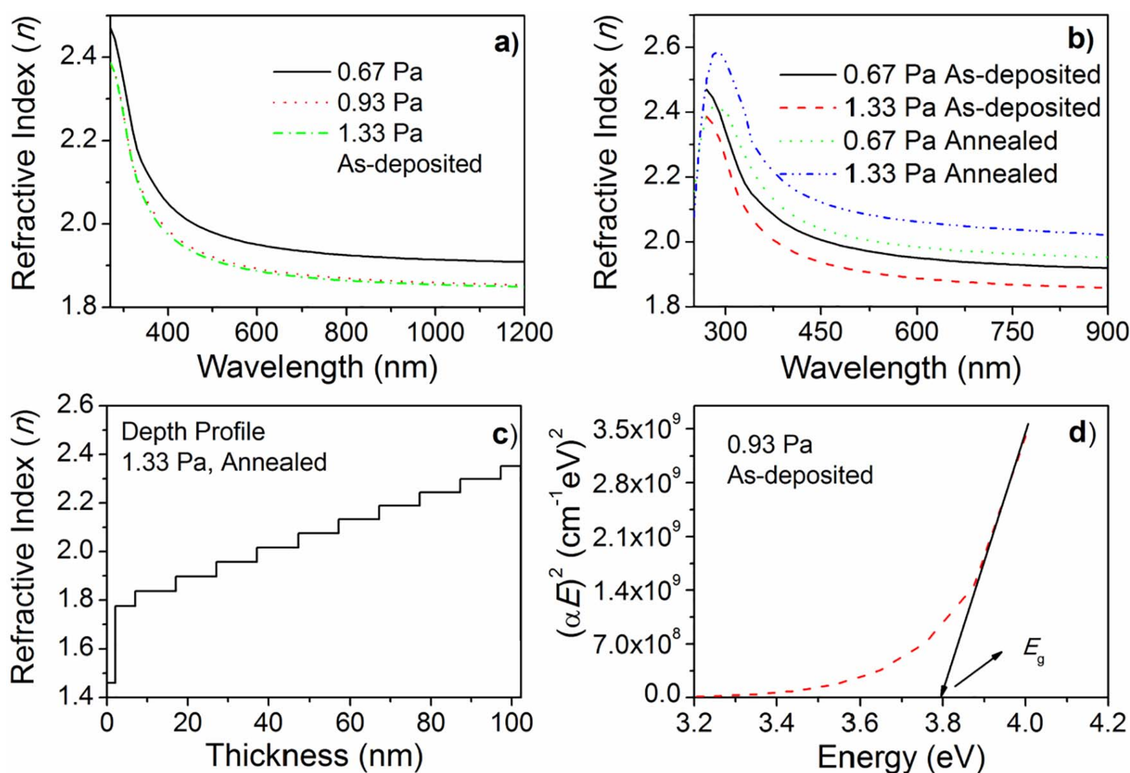

Fig. 7. (a) Spectral refractive index plots of as-deposited BST films. (b) Spectral refractive index plots of as-deposited and annealed BST thin films deposited at P_D = 0.67 and 1.33 Pa. (c) Refractive index depth profile for the annealed film.

Table 3
Refractive indices (n), extinction coefficients (k), and optical energy band gaps (E_g) of as-deposited and annealed BST thin films.

P_D (Pa)	As-deposited			Annealed		
	n (@ 550 nm)	k (@ 550 nm)	E_g (eV)	n (@ 550 nm)	k (@ 550 nm)	E_g (eV)
0.67	1.96	0.00	4.30	2.00	0.00	3.69
0.93	1.90	0.00	4.30	1.98	0.06	3.68
1.33	1.90	0.00	4.30	2.07	0.00	3.60

3.3. Electrical properties

Electrical characteristics, including frequency-dependent dielectric constant (ε and dielectric loss values of as-deposited and annealed BST thin films are presented in Fig. 9(a) and (b), respectively. In the present work, the dielectric constant values of film were evaluated for film thicknesses in the range 115 to 176 nm. Dielectric constants of the BST films were found to be low compared to the values reported for films deposited at higher temperatures in the literature. Average ε of the as-deposited films were between 46 and 53 (up to 800 kHz), and slightly increased with increasing frequency (Fig. 9(a)). Post-deposition annealing improved film dielectric constants. After the post-deposition annealing treatment, ε further increased and reached up to 66, 81, and 62 for films deposited at 0.67, 0.93, and 1.33 Pa chamber pressures, respectively.

Dielectric properties of the BST films depend on few factors including film thickness, composition and film stress. In general, ε values are thickness dependent and also more than an order of magnitude lower than its bulk form in thin films. In literature mostly thick films (thickness > a few hundred nanometers) shows high dielectric constant (ε_r > 300). In literature, the dielectric constant values of sputter deposited BST films on different substrates varied between 180 and 638 for ~500 nm thick films [1,24,39,40], while the dielectric constants of 400 nm spin coated $Ba_xSr_{1-x}TiO_3$ for two different x concentrations (0.4 and 0.8) were noted as 680 and 749, respectively [41]. Dielectric constant and leakage current were also noted as a function of oxygen mixing ratio by Tsai et al. [39]. They reported that the dielectric constant of ~50 for low deposition temperature and 400 for high deposition temperature (450 °C) at 50% oxygen mixing ratio. In addition to the low film thickness, the residual strains in BST thin films which were deposited on Si substrate may affect the dielectric constant of the film. Taylor et al. showed that the thermal expansion coefficient of the host substrate is affecting the dielectric constant of the grown thin films [42]. The dielectric permittivity decreased for the substrates which has lower thermal expansion coefficient [43].

In addition to the dielectric constant values, average dielectric loss and CSC values were calculated. The average loss values were found to be 0.02 for all as-deposited films independent of the sputtering conditions. However, for annealed films, the dielectric loss values increased to 0.04 within the same frequency range (see Fig. 9(b)). It should be noted that the dielectric losses, which were relatively low (i.e., < 0.05) up to 100 kHz, increased at high frequencies and reached to 0.25–0.30 for as-deposited films. The loss mechanism is one of the important phenomenons for tunable device applications, remarkably in microwave frequencies. The origins of the dielectric loss in the ferroelectric material are divided into two mechanisms in the literature: 1) intrinsic and 2) extrinsic loss. In this study, the origin of loss may come from the interaction of the applied AC field and phonon within the crystal lattice of the material. The theory of the loss mechanism is related to the energy of photon as known as "Planck-Einstein relation" $h\nu$, where ν is the frequency of AC field [44,45], is absorbed during thermal phonon collisions, which occupy higher energies as an intrinsic loss mechanism. In Table 4, ε_r and CSC values are summarized for all films. CSC values were calculated to be 0.25, 0.30, and 0.27 MV cm^{-1}, and 1.1, 1.2, and 1.3 μC cm^{-2} for as-deposited, and 0.30, 0.36, and 0.72 MV cm^{-1}, and 1.1, 2.5, and 3.9 μC cm^{-2} for annealed BST films as a function of P_D (0.67, 0.93, and 1.33 Pa), respectively.

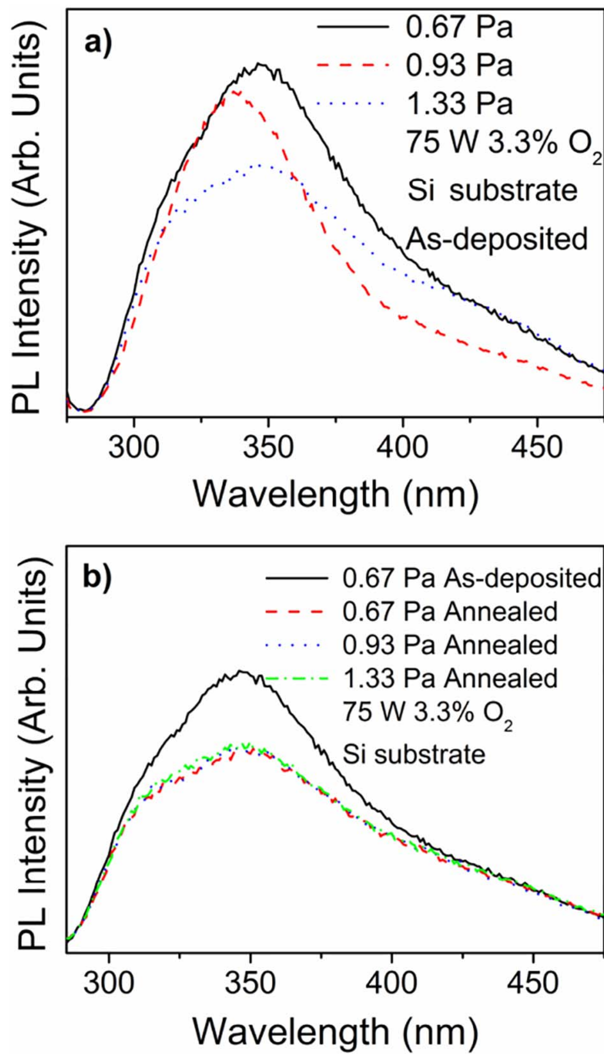

Fig. 8. PL emission spectra of (a) as-deposited, (b) annealed films as a function of wavelength.

Tuneable device applications require low dielectric loss factor (tanδ) and high dielectric tunability of the films. The performance of a tuneable dielectric material is generally evaluated using the FOM value, targeted to be as high as possible. The FOM value indicates that candidate material for tuneable device applications cannot take full advantage of high tunability if the loss tangent factor is too high. Our BST

Table 4
Dielectric constants (ε_r) at 100 kHz, and charge storage capacities (CSC) of as-deposited and annealed BST thin films.

P_D (Pa)		ε_r @ 100 kHz	CSC (μC cm^{-2})
0.67	*As-deposited*	47	1.1
	Annealed	66	1.8
0.93	*As-deposited*	49	1.2
	Annealed	81	2.5
1.33	*As-deposited*	53	1.3
	Annealed	62	3.9

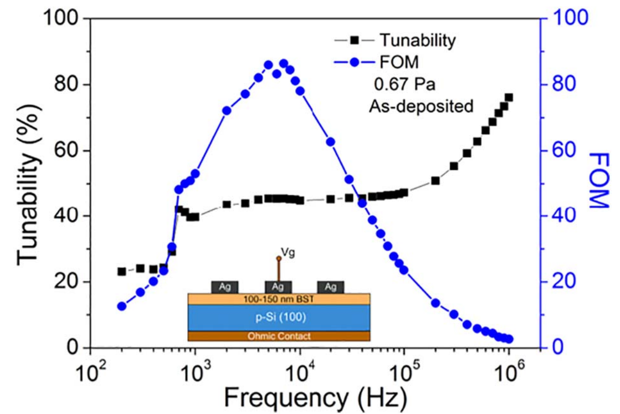

Fig. 10. Frequency dependent tunability and FOM values of Ag/BST/p-Si test structures (P_D = 0.67 Pa) fabricated using as-deposited BST thin films.

films deposited at 0.67 Pa pressure showed low dielectric constant, dielectric loss, and high FOM values. Tunability and FOM values of as-deposited films (P_D = 0.67 Pa) as a function of frequency are presented in Fig. 10. As can be seen from this figure, FOM reaches a maximum value of 86 (7 kHz). The FOM values of films deposited at 0.93 and 1.33 Pa pressures were 7 (9 kHz) and 19 (8 kHz). However, after annealing, their values increased to 48 (10 kHz) and 55 (8 kHz) while the value of film deposited at 0.67 Pa decreased to 36 (9 kHz). The observed differences might be originating from the varying film microstructure. It is known that in sputter technique the deposition pressure increase has positive effect on reducing the film stress. It should be noted that the XRD results indicated that the films deposited at high oxygen pressures had better crystallinity after annealing. Padmini et al. also stated higher tunability for films deposited at 550 °C using rf sputtering technique which was attributed to the improved texture of the BST films [46]. In addition, the change of tunability as a function of Ar/O_2 ratio is reported also by Pervez et al. [47]. They observed lower

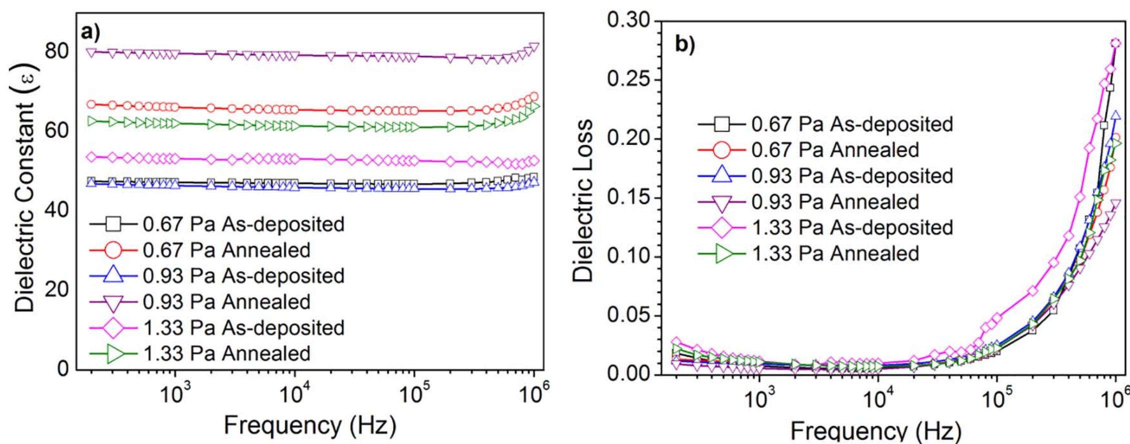

Fig. 9. (a) Frequency dependent dielectric constants and (b) dielectric loss values of Ag/BST/p-Si test structures (P_D = 1.33 Pa) fabricated using as-deposited and annealed BST thin films.

tunability values with the reduced (Ba + Sr)/Ti ratio changing from 1 to 0.78 with the increased O_2 pressure. We also observed similar effect as a function of (Ba + Sr)/Ti ratio.

Films deposited at 0.67 and 0.93 Pa showed higher average tunability values up to 100 kHz (41% and 53%) whereas the films deposited at 1.33 Pa had the lowest value of 18%. After annealing, the most pronounced change was for the BST films deposited at lower pressures < 1.33 Pa. Average tunability values of annealed films (up to 100 kHz) decreased to 26% and 16% for films deposited at 0.67 and 0.93 Pa, respectively. On the contrary, its value showed an increase and was 40% for annealed films deposited at 1.33 Pa.

4. Conclusion

Highly transparent, amorphous and well adhered films were deposited independent of the deposition pressure. Post-deposition annealing improved film crystallinity and significantly affected the optical and electrical characteristics of BST films. Annealed films showed cubic perovskite phase with no sub-phase formation, as well as exhibited a lower optical band gap, indicating an improved structure. The main effect was observed for films deposited at higher pressure. Electrical dielectric constants, CSC and tunability of films increased with deposition pressure upon annealing. Dielectric constant generally increases with thickness while thin films with < 200 nm thicknesses are favourable for microwave tunable devices.

Acknowledgment

Authors, E.G. and T.B. gratefully acknowledge the financial support from the Scientific and Technological Research Council of Turkey (TUBITAK) (Project #115F077 and #214M015). Authors would also like to acknowledge E. Kahveci for XPS, Dr. M. T. Guler for his assistance in electrical measurements, A. Haider and S. A. Leghari for their assistance in SEM and AFM measurements.

References

[1] K.H. Chen, C.M. Cheng, C.C. Lin, J.H. Tsai, Ferroelectric, dielectric, and physical characteristics of (Ba1 − xSrx)(Ti1 − yZry)O3 thin films, Integr. Ferroelectr. 143 (1) (2013) 32–39.
[2] S. Ezhilvalavan, T. Tseung-Yuen, Progress in the developments of (Ba,Sr) TiO3 (BST) thin films for gigabit era DRAMs, Mater. Chem. Phys. 65 (3) (2000) 227–248.
[3] E. Goldenberg, T. Bayrak, C. Ozgit-Akgun, A. Haider, S.A. Leghari, M. Kumar, N. Biyikli, Effect of O2/Ar flow ratio and post-deposition annealing on the structural, optical and electrical characteristics of SrTiO3 thin films deposited by RF sputtering at room temperature, Thin Solid Films 590 (2015) 193–199.
[4] A.K. Tagantsev, V.O. Sherman, K.F. Astafiev, J. Venkatesh, N. Setter, Ferroelectric materials for microwave tunable applications, J. Electroceram. 11 (1–2) (2003) 5–66.
[5] L.B. Kong, S. Li, T.S. Zhang, J.W. Zhai, F.Y. Chiang Boey, J. Ma, Electrically tunable dielectric materials and strategies to improve their performances, Prog. Mater. Sci. 55 (8) (2010) 840–893.
[6] A. Ahmed, I.A. Goldthorpe, A.K. Khandani, Electrically tunable materials for microwave applications, Appl. Phys. Rev. 2 (1) (2015) 011302.
[7] S. Li, Y. Yanqin, L. Liu, T.J. Zhang, W.H. Huang, Influence of deposition parameters on preferred orientation of RF magnetron sputtered BST thin films, J. Mater. Sci. Mater. Electron. 19 (3) (2008) 223–226.
[8] S.Z. Li, Y.Q. Yang, L. Liu, W.C. Liu, S.B. Wang, The preparation and refractive index of BST thin films, Phys. B Condens. Matter 403 (17) (2008) 2618–2623.
[9] H. Shen, G. Yanhong, Z. Peng, M. Jianhua, S. Jinglan, M. Xiangjian, C. Junhao, Effect of oxygen to argon ratio on properties of (Ba,Sr)TiO3 thin films prepared on LaNiO3/Si substrates, J. Appl. Phys. 105 (6) (2009) 061637.
[10] K. Saravanan, K. Venkata, M. Sudheendran, K. Ghanashyam, K.C. James Raju, Effect of the amorphous-to-crystalline transition in Ba0.5Sr0.5TiO3 thin films on optical and microwave dielectric properties, J. Phys. D. Appl. Phys. 42 (4) (2009) 045401.
[11] T.J. Zhang, S.Z. Li, B.S. Zhang, R.K. Pan, W.H. Huang, J. Jiang, Optical properties of RF magnetron sputtered Ba0.65Sr0.35TiO3 thin films, Ceram. Int. 33 (5) (2007) 723–726.
[12] Z. Jiwei, S. Bo, Y. Xi, Z. Liangying, Dielectric and ferroelectric properties of Ba (Sn0.15Ti0.85)O3 thin films grown by a sol–gel process, Mater. Res. Bull. 39 (11) (2004) 1599–1606.
[13] S. Regnery, P. Ehrhart, K. Szot, R. Waser, Y. Ding, C.L. Jia, M. Schumacher, T. Mcentee, MOCVD of (Ba,Sr)TiO3: nucleation and growth, Integr. Ferroelectr. 57 (1) (2003) 1175–1184.
[14] N. Scarisoreanu, M. Filipescu, A. Ioachim, M.I. Toacsan, M.G. Banciu, L. Nedelcu, A. Dutu, M. Buda, H.V. Alexandru, M. Dinescu, BST thin films obtained by PLD for applications in electronics, Appl. Surf. Sci. 253 (19) (2007) 8254–8257.
[15] M.M. Rutkowski, K. McNicholas, Z.Q. Zeng, F. Tuomisto, L.J. Brillson, Optical identification of oxygen vacancy formation at SrTiO3–(Ba,Sr)TiO3 heterostructures, J. Phys. D. Appl. Phys. 47 (25) (2014) 255303.
[16] V. Craciun, R.K. Singh, Characteristics of the surface layer of barium strontium titanate thin films deposited by laser ablation, Appl. Phys. Lett. 76 (14) (2000) 1932–1934.
[17] R. Thielsch, K. Kaemmer, B. Holzapfel, L. Schultz, Structure-related optical properties of laser-deposited BaxSr1 − xTiO3 thin films grown on MgO (001) substrates, Thin Solid Films 301 (1) (1997) 203–210.
[18] D.Y. Lei, S. Kéna-Cohen, B. Zou, P.K. Petrov, Y. Sonnefraud, J. Breeze, S.A. Maier, N.M. Alford, Spectroscopic ellipsometry as an optical probe of strain evolution in ferroelectric thin films, Opt. Express 20 (4) (2012) 4419–4427.
[19] R. Zhaodi, S. Mei, L. Weimin, H. Anhong, W. Defa, H. Gaorong, W. Wenjian, M. Ning, D. Piyi, B.S.T. Thin Film, Deposited on glass substrate with TISI nanowire electrode by RF-sputtering method, Ferroelectrics 387 (1) (2009) 167–174.
[20] V. Železný, D. Chvostová, L. Pajasová, M. Jelínek, T. Kocourek, S. Daniš, V. Valvoda, Temperature dependence of the optical properties of Ba0.75Sr 0.25TiO3 thin films, Thin Solid Films 571 (2014) 416–419.
[21] P. Shi, X. Yao, L. Zhang, Reactive ion etching of sol–gel-derived BST thin film, Ceram. Int. 30 (7) (2004) 1513–1516.
[22] Z. Xu, Y. Tanushi, M. Suzuki, K. Wakushima, S. Yokoyama, Optical properties of amorphous Ba0.7Sr0.3TiO3 thin films obtained by metal organic decomposition technique, Thin Solid Films 515 (4) (2006) 2326–2331.
[23] F. Challali, M.P. Besland, D. Benzeggouta, C. Borderon, M.C. Hugon, S. Salimy, J.C. Saubat, A. Charpentier, D. Averty, A. Goullet, J.P. Landesman, Investigation of BST thin films deposited by RF magnetron sputtering in pure argon, Thin Solid Films 518 (16) (2010) 4619–4622.
[24] X. Zhu, G. Le Rhun, B. Dkhil, Y. Ren, J. Zhu, M. Aïd, E. Defaÿ, Tailoring the room temperature ferroelectric/paraelectric state in polycrystalline (Ba0.70Sr 0.30) TiO3 thin films for silicon compatible integration, Ceram. Int. 41 (10) (2015) 14412–14418.
[25] Y. Xia, C. Cong, X. Zhi, B. Pan, D. Wu, X. Meng, Z. Liu, Effects of the substitution of Pb for Ba in (Ba, Sr) TiO3 films on the temperature stability of the tunable properties, Appl. Phys. Lett. 88 (18) (2006) 182909.
[26] D.Y. Noh, H.H. Lee, T.S. Kang, J.H. Je, Crystallization of amorphous (Ba,Sr)TiO3/MgO (001) thin films, Appl. Phys. Lett. 72 (22) (1998) 2823–2825.
[27] W.J. Lee, I.K. Park, G.E. Jang, H.G. Kim, Electrical properties and crystal structure of (Ba0.5Sr0.5)TiO3 thin films prepared on Pt/SiO2/Si by RF magnetron sputtering, Jpn. J. Appl. Phys. 34 (1R) (1995) 196.
[28] Sanjeeb Kumar Rout, Phase Formation and Dielectric Studies of Some BaO-TiO_2-ZrO_2 Based Perovskite System, PhD diss. (2006).
[29] T. Zhang, G. Haoshuang, J. Liu, Structural and optical properties of BST thin films prepared by the sol–gel process, Microelectron. Eng. 66 (1) (2003) 860–864.
[30] Y.F. Kuo, T.Y. Tseng, Structure-related optical properties of rapid thermally annealed Ba0.7Sr0.3TiO3 thin films, Mater. Chem. Phys. 61 (3) (1999) 244–250.
[31] S.B. Singh, H.B. Sharma, H.N.K. Sarma, S. Phanjoubam, Influence of crystallization on the spectral features of nano-sized ferroelectric barium strontium titanate (Ba0.7Sr0.3TiO3) thin films, Phys. B Condens. Matter 403 (17) (2008) 2678–2683.
[32] A. Fikadu, A. Reinholz, K. Pokhodnya, Stoichiometry and phase purity control of radio frequency magnetron sputter deposited Ba0.45Sr0.55TiO3 thin films for tunable devices, J. Appl. Phys. 114 (17) (2013) 174104.
[33] S.C. Roy, G.L. Sharma, M.C. Bhatnagar, Large blue shift in the optical band-gap of sol–gel derived Ba0.5Sr0.5TiO3 thin films, Solid State Commun. 141 (5) (2007) 243–247.
[34] B. Panda, A. Dhar, G.D. Nigam, D. Bhattacharya, S.K. Ray, Optical properties of RF sputtered strontium substituted barium titanate thin films, Thin Solid Films 332 (1) (1998) 46–49.
[35] A. David, S. Guérin, B.E. Hayden, R. Noble, J.P. Soulié, C. Vian, I.P. Koutsaroff, S.I. Higai, N. Tanaka, T. Konoike, A. Ando, High-throughput synthesis and characterization of (BaxSr1 − x)1 + yTi1 − yO3 − δ and (BaxSr1 − x) 1 + yTi1 − yO3 − zNz perovskite thin films, Cryst. Growth Des. 14 (2) (2014) 523–532.
[36] P.S. Pizani, E.R. Leite, F.M. Pontes, E.C. Paris, J.H. Rangel, E.J.H. Lee, E. Longo, P. Delega, J.A. Varela, Photoluminescence of disordered ABO3 perovskite, Appl. Phys. Lett. 77 (6) (2000) 824–826.
[37] A.E. Souza, G.T.A. Santos, B.C. Barra, W.D. Macedo Jr., S.R. Teixeira, C.M. Santos, A.M.O.R. Senos, L. Amaral, E. Longo, Photoluminescence of SrTiO3: influence of particle size and morphology, Cryst. Growth Des. 12 (11) (2012) 5671–5679.
[38] I.A. Souza, M.F.C. Gurgel, L.P.S. Santos, M.S. Góes, S. Cava, M. Cilense, I.L.V. Rosa, C.O. Paiva-Santos, E. Longo, Theoretical and experimental study of disordered Ba0.45Sr0.55TiO3 photoluminescence at room temperature, Chem. Phys. 322 (3) (2006) 343–348.
[39] M.S. Tsai, S.C. Sun, T.Y. Tseng, Effect of oxygen to argon ratio on properties of (Ba,Sr)TiO3 thin films prepared by radio-frequency magnetron sputtering, J. Appl. Phys. 82 (7) (1997) 3482–3487.
[40] B.A. Baumert, L.H. Chang, A.T. Matsuda, T.L. Tsai, C.J. Tracy, R.B. Gregory, P.L. Fejes, N.G. Cave, W. Chen, D.J. Taylor, T. Otsuki, E. Fujii, S. Hayashi, K. Suu, Characterization of sputtered barium strontium titanate and strontium titanate-thin films, J. Appl. Phys. 82 (5) (1997) 2558–2566.
[41] F.M. Pontes, E. Longo, E.R. Leite, J.A. Varela, Study of the dielectric and ferroelectric properties of chemically processed BaxSr1 − xTiO3 thin films, Thin Solid Films 386 (1) (2001) 91–98.
[42] T.R. Taylor, P.J. Hansen, B. Acikel, N. Pervez, R.A. York, S.K. Streiffer, J.S. Speck,

Impact of thermal strain on the dielectric constant of sputtered barium strontium titanate thin films, Appl. Phys. Lett. 80 (11) (2002) 1978–1980.
[43] N.A. Pertsev, A.G. Zembilgotov, A.K. Tagantsev, Effect of mechanical boundary conditions on phase diagrams of epitaxial ferroelectric thin films, Phys. Rev. Lett. 80 (9) (1998) 1988.
[44] K. Przibram, E. Schrödinger, A. Einstein, H.A. Lorentz, M. Planck, Letters on Wave Mechanics, Philosophical Library, New York, 1967.
[45] W. Qin, Y. Guo, B. Guo, M. Gu, Dielectric and optical properties of BiFeO3–(Na0.5Bi0.5)TiO3 thin films deposited on Si substrate using LaNiO3 as buffer layer for photovoltaic devices, J. Alloys Compd. 513 (2012) 154–158.
[46] P. Padmini, T.R. Taylor, M.J. Lefevre, A.S. Nagra, R.A. York, J.S. Speck, Realization of high tunability barium strontium titanate thin films by rf magnetron sputtering, Appl. Phys. Lett. 75 (20) (1999) 3186–3188.
[47] N.K. Pervez, P.J. Hansen, R.A. York, High tunability barium strontium titanate thin films for rf circuit applications, Appl. Phys. Lett. 85 (19) (2004) 4451–4453.